

FINAL TECHNICAL REPORT

Paleoseismology of the Promontory Segment, East Great Salt Lake Fault

U.S. Geological Survey Award Number 02HQGR0105

by

David A. Dinter and James C. Pechmann
University of Utah
Department of Geology and Geophysics

Period of Award (with no-cost extensions):
July 1, 2002 to June 30, 2007

Principal Investigators
David A. Dinter and James C. Pechmann
University of Utah
Department of Geology and Geophysics
115 South 1460 East Room 383 FASB
Salt Lake City, UT 84112-0102
Tel: 801-581-7937 (DAD); 801-581-3858 (JCP)
Fax: 801-581-7065 (DAD); 801-585-5585 (JCP)
E-mail: david.dinter@utah.edu; pechmann@seis.utah.edu

Report Date: August 25, 2014

Research supported by the U.S. Geological Survey (USGS), Department of the Interior, under USGS award number 02HQGR0105. The views and conclusions contained in this document are those of the authors and should not be interpreted as necessarily representing the official policies, either expressed or implied, of the U.S. Government.

ABSTRACT

With funding from this project, we collected 367 km of high resolution seismic reflection data in the Great Salt Lake in 2003 and 2006: 205 km in the north arm and 162 km in the south arm, where the north and south arms are defined as the parts of the lake north and south of the railroad causeway, respectively. Because the quality of the north arm data that we obtained was insufficient to meet the goals of the project, we collected an additional 380 km of data with new, state-of-the-art instrumentation in 2009 and 2010: 160 km in the north arm and 220 km in the south arm. The 2009 fieldwork was part of a collaborative industry-funded study. The 2010 fieldwork was carried out using boat and equipment time that became available after the successful completion of a seismic reflection study in Utah Lake for another USGS/NEHRP-funded study.

We used the seismic reflection data to map the Great Salt Lake fault (GSLF) and associated subsidiary faults in the north arm of the Great Salt Lake and to revise an analogous map for the south arm of the lake that we constructed for a previous USGS/NEHRP-funded project. We also mapped the trace of the Carrington fault, another major normal fault in the Great Salt Lake, using our seismic reflection data and high-resolution bathymetry data for the lake. Based on the geometry of our mapped surface trace for the GSLF, variations in the amount of lakebed offset along this fault, and other evidence for recency of faulting, we hypothesize that the GSLF consists of the following four segments from north to south (with end-to-end length measurements): the Rozel segment (≥ 18 km), the Promontory segment (≥ 27 km), the Fremont Island segment (24 km), and the Antelope Island segment (35 km).

Seismic reflection profiles across the GSLF in the north arm show clear evidence for individual paleoearthquakes in the form of stratigraphically limited subsidiary faults and monoclines and coseismic bedding rotations adjacent to the fault. Based on these types of features, we have identified seismic event horizons for two or three paleoearthquakes on the Rozel segment and two or three paleoearthquakes on the Promontory segment, all within ~ 8 m of the lake bottom. A possible fourth Promontory segment earthquake is suggested by the higher fault scarps along this segment. The earthquake event horizons that we have identified in this study can be cored and dated to establish a paleoearthquake history for the Rozel and Promontory segments of the GSLF. In the meantime, based on comparisons with the depths of dated event horizons on the Antelope Island and Fremont Island segments, it seems reasonable to assume that the average recurrence interval of 4200 ± 1400 years that we have determined for these two segments is also applicable to the Rozel and Promontory segments.

INTRODUCTION

The Great Salt Lake fault (GSLF), formerly known as the East Great Salt Lake fault, is a major west-dipping normal fault submerged beneath the Great Salt Lake 10-30 km west of the Ogden-Salt Lake City metropolitan area and 30-70 km west of the Wasatch fault (Figure 1). The GSLF strikes south-southeast along the western boundary of a discontinuous topographic high defined, from north to south, by the Promontory Mountains and Fremont and Antelope Islands in the Great Salt Lake. Multichannel seismic reflection data collected by Amoco in the late 1970s show that the GSLF forms the eastern boundary of a large Cenozoic half graben in which the sedimentary fill dips and thickens eastward (Smith and Bruhn, 1984; Bortz et al., 1985; Viveiros, 1986; Mohapatra and Johnson, 1998). The deepest part of the basin contains more than 4000 m of post-Oligocene sedimentary strata (Bortz et al., 1985; Mohapatra and Johnson, 1998), indicative of major subsidence during the past 23 m.y. Well data and high resolution seismic reflection profiles show that the GSLF displaces Quaternary (Mikulich and Smith, 1974; Viveiros, 1986) and Holocene (Colman et al., 2002; Dinter and Pechmann, 2005) deposits and must therefore be considered active.

There is good evidence for another major normal fault in the Great Salt Lake. This northwest-dipping fault, named the Carrington fault, follows the northwestern edge of a structural and topographic high that extends southwestward from the southern end of the Promontory Mountains (Figure 1; Mohapatra and Johnson, 1998; Colman et al., 2002). This topographic high divides the Great Salt Lake west of the GSLF into two large sedimentary basins (Bortz et al., 1985).

In work funded by two previous USGS/NEHRP awards, we investigated the GSLF and associated subsidiary faults in the south arm of the Great Salt Lake. The south and north arms of the lake are, respectively, the parts of the lake located south and north of the Southern Pacific Railroad causeway (Figures 1 and 2). In the first phase of our previous work we mapped the faults in the south arm using high resolution seismic reflection data that we collected in 1998, supplemented by similar data collected by S.M. Colman and K.R. Kelts in 1997 (Colman et al., 2002). Our map of the GSLF in the south arm from this study, shown on Figure 1, shows a 2-km left step in the active trace west of northern Antelope Island. Based on lakebed offsets and other evidence for recency of faulting, we interpreted this left step as a boundary separating the fault south of the Promontory Mountains into two segments: a 35-km-long Antelope Island segment and a 30-km-long Fremont Island segment (where the segment length measurements are end-to-end). The trace of the GSLF shown in the north arm on Figure 1 is from a map of the GSLF that we constructed using Amoco airgun data. The division of the GSLF in the north arm into the two segments shown on this map is based on preliminary work on the project that is the subject of this report.

The most exciting and useful discovery from our 1998 seismic survey was unambiguous tectonostratigraphic evidence for individual paleoearthquakes. This evidence consists of coseismic bedding rotations, associated onlap surfaces and angular unconformities, and stratigraphically limited subsidiary faults imaged in post-Bonneville (post-13.5 ka) hanging-wall deposits. These features delineate event horizons associated with the three most recent earthquakes on each of the two GSLF segments in the south arm (Dinter and Pechmann, 2005).

The second phase of our previous work consisted of the collection of lake sediment cores in 2000 at two different sites along the GSLF that were selected based on our 1998 seismic reflection data. The core collection was funded by the National Science Foundation as part of a collaborative study with a group of University and U.S. Geological Survey (USGS) paleoclimatologists. The third phase of the work utilized the cores and the seismic reflection data to date individual paleoearthquakes and determine an average single-segment recurrence interval of 4200 ± 1400 years (2 sigma error bars) for large, surface-faulting earthquakes on the Fremont Island and Antelope Island segments of the GSLF (Dinter and Pechmann, 2005).

In this report, we summarize the work performed and the results obtained with our third USGS/NEHRP grant for studies of faults beneath the Great Salt Lake. The primary emphasis in this project was on seismic reflection studies of the GSLF and related faults in the north arm of the Great Salt Lake. However, we also collected and interpreted some additional seismic reflection data from the south arm of the lake—in part because of equipment and logistical problems that we encountered while trying to acquire seismic reflection data in the north arm of the lake.

FIELDWORK

The fieldwork for this project was extremely challenging due to unexpected logistical and equipment problems, most of which were related to the harsh, hypersaline environment of the north arm of the Great Salt Lake. It ultimately took us four field seasons, spread out over a time period of eight years, to acquire data of sufficient quality and quantity to meet all of the goals of the project. These data were acquired during the summers of 2003, 2006, 2009, and 2010. We carried out the last two of these field campaigns after the no-cost extensions and funding for this award ended in 2007. The map in Figure 2 shows the locations of the seismic reflection profiles collected during these four years and during our previous USGS/NEHRP-funded project in 1998. This map also shows the locations of seismic reflection profiles collected by S.M. Colman and K.R. Kelts in 1997 that we have used in our research (Colman et al., 2002).

In order to explain the problems that we encountered during the fieldwork, we begin with some background information on the north arm of the Great Salt Lake. As mentioned previously, the Great Salt Lake is divided into two parts, called the north arm and the south arm, by the Southern Pacific Railroad causeway. This causeway is a rock-fill structure that spans the lake between the western shore and Promontory Point, which is located at the southern end of the Promontory Mountains (Figure 2). This causeway forms a complete navigational barrier and a nearly complete mixing barrier between the north and south arms of the lake. Because of this barrier, and because ~95% of the stream flow into the lake enters the south arm, the water in the north arm is more than three times as saline as that of the south arm (White et al., 2014). The salinity of the north arm is often at or near the saturation level of 317 g/l (White et al., 2014), which is nine times the salinity of seawater.

Boat access to the south arm is available from two marinas with concrete boat ramps (Figure 2). The closest marina to Salt Lake City, and the one where the USGS boat used for the 2003 and 2006 fieldwork is stored, is a 34 km (21 mile) drive from the University of Utah on the

south shore. Boat access to the north arm is from Little Harbor on the southwestern edge of the Promontory Mountains, a small artificial harbor that was dredged to support oil exploration activities on the lake during the 1970s (Figure 2). This harbor has been equipped with a concrete boat ramp since 2004. Little Harbor is a 182 km (113 mile) drive from the University of Utah on public roads, with the last 53 km (33 miles) on unpaved roads.

During the first year of the award, 2002, we were unable to collect any data for this study because precipitation of salt crystals in the north arm of the lake prevented the use of outboard motors. The salt crystals clog the filters on outboard motor cooling systems, which use lake water as the coolant.

On June 28, 2003, we began our fieldwork with seismic reflection equipment borrowed from a USGS office in Connecticut and a boat from the USGS Water Resources Division Office in Salt Lake City. We initially deployed this equipment in the south arm of the lake for testing and optimization. Because of unanticipated problems with a new upgrade to the Triton Elics, Inc., Delph Seismic data acquisition software that was supplied to us with the USGS seismic equipment, the testing and debugging period occupied some 10 days. Nevertheless, during this time period we successfully acquired 150 km of seismic reflection data in the south arm to supplement the data that we had collected in 1998. After the boat and the equipment were moved to the north arm, mechanical problems with operating the USGS boat motors in the hypersaline north arm forced us to abandon the fieldwork after only two days of successful data collection. During those two days, which were separated in time by more than a month of work on the boat motors, we acquired ~75 km of seismic profiles. The boat motor problem was not fixed until early 2004, when the motors were modified to fix a design flaw that caused them to fail under the demanding conditions of seismic data collection in the north arm.

By the summer of 2004, due to several years of drought, the lake level had dropped so low that it was no longer possible to launch boats of the size that we needed from the soft sand beach at Little Harbor. Because Little Harbor is the only large boat launch site available on the north arm of the lake, and is an important facility for the brine shrimp industry, the State of Utah built a concrete boat ramp there in 2004 to enable boat launches in low water conditions. However, by the time that this boat ramp opened for use on October 25, it was too late in the year for us to undertake another data collection expedition.

During the summer of 2006, using the same seismic reflection equipment and boat as in 2003, we were able to collect 130 km of seismic data in the north arm and an additional 12 km of data in the south arm. In order to successfully operate the boat in the north arm, we had to pull it out of the water every 1-2 days to remove the salt buildup from the motors. This maintenance slowed down the data collection, but was necessary to prevent boat motor failures. The same maintenance procedures were necessary during our 2009 and 2010 fieldwork, which was carried out using a different boat.

Unfortunately, much of the 206 km of data collected in the north arm in 2003 and 2006 turned out to be of marginal quality. We suspect that these data quality problems were caused by a combination of the following three factors: (1) a layer of salt on the lake bottom in most of the north arm, which absorbed much of the seismic energy produced by the sources that we were using, (2) salt damage to the instrumentation, and (3) electronic interference between the Global

Positioning System (GPS) device used for navigation and the seismic data acquisition system.

While we were attempting to analyze our less-than-optimal data from the north arm, we were offered an opportunity to collect some additional data in the north arm using new, state-of-the-art marine seismic reflection equipment developed at the Scripps Institute of Oceanography. We collected these additional data in 2009 in collaboration with Robert Baskin of the USGS Water Resources Division Office in Salt Lake City who was conducting a study of the effects of faults on stromatolite distributions in both the north and south arms (Baskin, 2014). Baskin's study was funded by the BG Group, a British oil and gas company. The 2009 Great Salt Lake data are owned by the BG Group and are used here with their permission.

Finally, during 2010 we obtained more data in the north arm using the same Scripps seismic reflection equipment that we used in 2009. We brought this equipment to Utah in 2010 for a USGS/NEHRP-funded study of faults beneath Utah Lake. Because the fieldwork for the Utah Lake study finished ahead of schedule, we were able to deploy the equipment in the north arm of the Great Salt Lake in areas where our previous data coverage was insufficient. In total, during 2009 and 2010 we collected 380 km of high resolution seismic data with the Scripps system: 160 km in the north arm and 220 km in the south arm. The 2009 and 2010 data were by far the best data that we obtained for this project due to the superior capabilities of the Scripps system. The 2009 and 2010 data are the only data from the north arm on which we have been able to identify seismic event horizons. These data were also of critical importance for our mapping of the Great Salt Lake fault in the north arm of the lake. In short, the results presented in this report rely heavily on the data that we collected in 2009 and 2010, in part with private funding, after the time period of this award had ended.

DATA COLLECTION

During our 2003 and 2006 surveys, the seismic sources and hydrophones were towed from a 27-foot cathedral-hull USGS-owned research boat with twin 170-HP marine motors at speeds ranging from 4-8 km/hr. Two seismic sources were operated simultaneously: (1) an Edgetech SB-216S high-frequency Compressed High Intensity Radar Pulse (Chirp) subbottom profiler and (2) a Geopulse boomer, towed from opposite sides of the survey vessel and triggered at identical 0.5-sec intervals. Data were digitized and written to a hard disk in SEG-Y format using Triton Elics hardware and Delph SeismicPlus software. Chirp transducers and hydrophones housed in a single towfish were towed ~1 meter beneath the lake surface. The transducers sweep a 2-7-kHz frequency range in 0.005 s, typically producing good images of unconsolidated lake sediments as deep as 15-20 m below the lakebed. The Geopulse boomer plate assembly was towed on a catamaran ~0.25 m below the lake surface, and produced energy primarily in the 800-3000 Hz range. The Geopulse hydrophone streamer was towed ~2 m forward of the source at the same depth, but on the opposite side of the hull. Operating at 200 Joules, this system commonly images strata to 75 m below the lakebed, exceptionally as deep as 150 m. A 12-channel Trimble ProXR GPS system was employed for real-time navigation and trackline locations accurate to ± 10 m.

The seismic reflection equipment that we used during our 2009 and 2010 surveys was a custom-built Chirp system on loan from the Scripps Institute of Oceanography and designated as an Edgetech SB512SC (see Baskin, 2014). The Chirp towfish contains both the seismic source and receiver. Two transducers on the towfish supply an outgoing Chirp signal in two overlapping frequency ranges, with one producing a signal from 500 Hz to 6 kHz and the other from 2-16 kHz. In our surveys, we configured the transducers to sweep a 0.7-3 kHz frequency range in 0.05 s or a 1-15 kHz frequency range in 0.03 s, with a time interval of 0.5 s between sweeps and a recording time of 0.133 s. The receiver in the towfish consists of four hydrophone arrays in a near vertical orientation, the output of which is summed to produce a single record from each outgoing source pulse. The known Chirp source signal is deconvolved from each record as part of the data acquisition process. Under optimal conditions, the SB512SC Chirp system can obtain interpretable data to ~30 m below the lakebed. Position information during the 2009 and 2010 surveys was supplied by a GPS receiver supplemented with a Wide Area Augmentation System (WAAS) capable of providing ± 3 m accuracy 95% of the time.

The Edgetech SB512SC differs from commercial units in that the signal digitization and source deconvolution processes are done in an on-fish pressured bottle instead of in a computer on the boat. This configuration minimizes interference from electromagnetic sources and reduces variations in signal quality resulting from environmental conditions. The data are recorded on hard disk in an Edgetech format. We later converted the data to SEG-Y format.

We imported all of the SEG-Y format data collected for this project into the format used by the IHS Kingdom Suite software package, which we used for viewing and interpreting the data.

FAULT MAPS

We mapped the surface traces of the GSLF and associated subsidiary faults in the north arm using data from the seismic reflection tracklines shown in Figures 2 and 3 (Figure 3). The main traces of the GSLF and the Carrington fault are shown in a heavier line width than the subsidiary fault traces on the fault map in Figure 3. The color coding for the faults is indicative of the relative age of the youngest sediments affected by the faulting, either by direct displacement or by monoclinical folding above the tip of the fault. The faults shown in red displace the lake bottom. The faults shown in green deform sediments within ~0.01 sec two-way travel time (TWTT) of the lake bottom. This TWTT corresponds to a depth of ~8.5 m based on an average shallow sediment velocity of 1700 m/s determined from sonic logs obtained in 2000 at one of the coring sites. The faults shown in blue deform sediments below ~0.01 s TWTT only. The TWTT of 0.01 sec was chosen to emulate a different relative age classification for the faults that we used in the south arm. For the south arm faults on Figures 3 and 4, the green color indicates offsets or folding of sediments above a reflector that we have designated H_0 . The blue color indicates that such deformation is restricted to sediments below H_0 . H_0 is a strong early Holocene reflector that is traceable in most of the south arm but cannot be confidently identified on the north arm seismic reflection data.

We have mapped the GSLF in the north arm as consisting of four separate strands separated by left steps (Figures 3 and 5). There is a lake bottom fault scarp present along the entire length

of the GSLF in the north arm, but it is smaller on the two northern strands over most of their lengths. The extension of the GSLF northwest of the trackline coverage was mapped on the basis of an east-northeast-trending Amoco seismic reflection line, located at the northern end of our mapped fault trace. We found no evidence for the GSLF on another east-northeast-trending Amoco line located 8 km north-northwest of the end of our mapped fault trace. Similarly, we found no evidence of the GSLF on our own seismic reflection lines located 10-15 km north-northwest of the end of our mapped GSLF fault trace (Figure 3). Consequently, although the northwestern extent of the GSLF is poorly known, it appears that it does not extend all the way to the north shore of the Great Salt Lake. Similarly, the distance that the GSLF strand on the west side of the Promontory Mountains extends northward into Rozel Bay is unknown due to the lack of data in this bay. Rozel Bay was inaccessible with our boats due to shallow water depths at the times of our surveys.

On Figure 5, we have superimposed our map of the GSLF on a bathymetry map for the north arm from Baskin and Turner (2006; see also Baskin, 2006). Figure 5 shows that our mapped surface trace for the GSLF in the north arm closely follows a distinct, west-facing, topographic escarpment located near the eastern shore of the lake. The seismic reflection data clearly show that this topographic escarpment is a fault scarp over much of its length. Our mapped fault trace deviates from the lake bottom escarpment north of about $41^{\circ} 28' N$.

In addition to mapping faults in the north arm of the Great Salt Lake, we used the seismic reflection data acquired in 2003 to revise our fault map for the south arm of the lake (Figures 4 and 6). In particular, the 2003 data allowed us to: (1) revise the map of the GSLF in the northern half of the south arm, including the complex stepover zones between the Antelope Island and Fremont Island segments and between the Fremont Island segment and the Promontory segment to the north (compare Figures 1 and 6); (2) map the active trace of the Carrington fault; and (3) revise and expand the map of subsidiary faults, including some with lake bottom scarps at the southern end of the lake.

Figure 6 shows our revised fault map for the south arm of the Great Salt Lake superimposed on a detailed bathymetry map for the south arm by Baskin and Allen (2005; see also Baskin, 2005). As in the north arm, our mapped trace of the GSLF in the south arm follows a prominent west-facing escarpment on the lake floor over much, but not all, of its length. The Carrington fault is also marked by a prominent lake floor escarpment. We used the location of this escarpment on the bathymetry map to extend our map of the Carrington fault well to the southwest of the available trackline coverage (Figures 4 and 6). At the northeastern end of the Carrington fault, a rapid decrease in displacement towards the end of our mapped fault trace implies that this fault does not merge with the Promontory segment of the GSLF as previously thought (e.g., Mohapatra and Johnson, 1998; Colman et al., 2002).

SEGMENTATION MODEL

Previously, we had divided the GSLF into three segments that we called, from south to north, the Antelope Island, Fremont Island, and Promontory segments (Figure 6). Based on our new data, we have subdivided the Promontory segment into two segments: the Promontory

segment on the south and the Rozel segment on the north, with the boundary between them located at Rozel Bay (compare Figures 1 and 5). The lengths of these segments, as measured end-to-end on our fault map, are ≥ 27 km for the Promontory segment and ≥ 18 km for the Rozel segment. Both segment lengths are minimum lengths because the locations of their northern ends are poorly constrained by the available data.

The basis for the subdivision of the GSLF north of Promontory Point into two segments is (1) the larger lake bottom scarp heights south of Rozel Bay, (2) the ~ 4 km left step in the fault trace at Rozel Bay, and (3) the change in the average fault strike from approximately south in the part of the fault south of Rozel Bay to southeast in the part of the fault north of Rozel Bay. We have also moved the boundary between the Promontory and Fremont Island segments farther south, based primarily on the amount of lake bottom displacement observed. Given the discontinuous nature of the GSLF in the vicinity of this segment boundary, the exact location of this boundary is somewhat uncertain.

The seismic hazard significance of our revised segmentation model is that it essentially doubles the expected frequency of large, surface-faulting earthquakes along the GSLF in the northern arm of the Great Salt Lake. Our revised segmentation model has been adopted by the Working Group on Utah Earthquake Probabilities (Wong et al., 2011) for use in calculating earthquake probabilities for the Wasatch Front region of Utah. We expect that this model will also be adopted for most future seismic hazard analyses in this region. Table 1 shows the lengths of the GSLF segments in our current segmentation model along with estimated moment magnitudes for surface faulting earthquakes on these segments. The latter are from two empirical relations between linear surface rupture length and moment magnitude for normal-faulting earthquakes: Wells and Coppersmith (1994) and Wesnousky (2008).

Segment Name	End-To-End Length (km)	Estimated Moment Magnitude	
		Wells and Coppersmith (1994)	Wesnousky (2008)
Rozel	≥ 18	≥ 6.5	≥ 6.7
Promontory	≥ 27	≥ 6.7	≥ 6.8
Fremont Island	24	6.7	6.8
Antelope Island	35	6.9	6.8

SEISMIC REFLECTION EVIDENCE FOR PALEOEARTHQUAKES

Figures 7-10 are examples of good-quality seismic reflection images from the north arm showing the GSLF, the surrounding lake sediments, and associated subsidiary faults and monoclines. The figures are labeled with the line names, which begin with two-digit numbers indicating the year that the data were acquired. The locations of the profiles in Figures 7-10 are

shown on Figure 3 as FC1 through FC4. Two of these profiles cross the southern strand of the Rozel segment, one is from the northernmost strand of the Promontory segment, and one is from the central (and longest) strand of the Promontory segment. Clear lake bottom scarps are evident on all four sample profiles. On three of the four profiles (all from 2010), there is tectonostratigraphic evidence in the hanging wall sediments for one or more surface faulting earthquakes. In all, we found such evidence on nine seismic reflection profiles crossing the GSLF in the north arm, and possible evidence on two more profiles.

Figure 7 shows the data from line 10GSL44 where it crosses the southern strand of the Rozel segment just west of Rozel Bay (Figure 3). The stratigraphic geometries of the hanging wall sediments at this location record at least two, and probably three, discrete surface ruptures on the GSLF. The youngest event occurred at the stratigraphic horizon labeled EH-R1, as indicated by the tilting of beds at and below this horizon toward the GSLF at distances of less than 70 m from the fault. The overlying beds dip less steeply toward the fault or in the other direction, onlapping the EH-R1 event horizon progressively to the southwest. Analogous tilted bedding structures deeper in the section provide evidence for additional paleoearthquake event horizons at EH-R3 and probably EH-R2, although the evidence for the latter is less clear. Further support for the occurrence of a paleoearthquake shortly after the deposition of EH-R1 comes from the southwest (left) side of the seismic reflection image in Figure 7. Here, monoclinical folding above two subsidiary faults affects beds at and below EH-R1. The beds overlying EH-R1 are relatively flat lying above the subsidiary faults. West of the subsidiary faults, the beds above EH-R1 appear to onlap the EH-R1 monoclinical surface.

Figure 8 shows an example of a GSLF crossing imaged in 2006 with the high-frequency Chirp system. This fault crossing is near the southern end of the Rozel segment. The GSLF and its associated lakebed scarp are clearly visible. However, the hanging wall sediments are not resolved well enough to show event horizons, if present.

Figure 9 shows the data from line 10GSL06 where it crosses the northern strand of the Promontory segment. Monoclinical folding of hanging wall sediments at and below horizon EH-P1 is clearly related to slip on an underlying subsidiary fault, recording the occurrence of a relatively recent earthquake on the GSLF at this location. The sediments above EH-P1 are unfolded and appear to onlap the monocline surface. Similar shallow (< 1.5 m) monocline termination surfaces are found at comparable depths on six other reflection profiles across the northern strand of the Promontory segment, all located within 3 km of each other. These monocline termination surfaces provide consistent evidence for a relatively recent earthquake on the Promontory segment. It is unclear if this earthquake is the same one that formed the prominent lake bottom scarp that is present along most of the length of this segment.

Finally, Figure 10 shows the data from line 10GSL 32 where it crosses the southern strand of the Promontory segment. The hanging wall sediments imaged on this line show the tectonostratigraphic signatures of two paleoearthquakes. Two subsidiary fault terminations indicate an event horizon at EH-P2. Apparent bedding rotations adjacent to the GSLF suggest a possible older event horizon at EH-P3. However, the presence of diffractions in the reflection data around these apparent bedding rotations introduce some uncertainty into this interpretation. Event horizons EH-P3 (if real) and EH-P2 are both several meters deeper below the lake bottom than EH-P1, indicating that they correspond to older events. Taken together, the hanging wall

sediments imaged on Figures 9 and 10 indicate at least two and probably three paleoearthquakes on the Promontory segment.

In summary, Figures 6-10 show evidence for two or three paleoearthquakes on the Rozel segment and two or three on the Promontory segment, with a possible fourth Promontory segment event suggested by the higher fault scarps along this segment. On the Rozel segment, evidence for the two or three paleoearthquakes is observed on a single line in the uppermost 7 m of lake sediments. On the Promontory segment, only two of the possible earthquake event horizons identified can be seen on any one line, but all are within the uppermost 8 m of the lake sediments. For comparison, we identified and dated three earthquake event horizons in the uppermost 6-9 m of lake sediments (depending where it is measured) on the Antelope Island segment and another three event horizons in the uppermost 14 m of sediment on the Fremont Island segment (Dinter and Pechmann, 2005). The sediments with the identified event horizons on the two southern segments of the GSLF are all of Holocene age ($< 11,427 \pm 605/-449$ B.P.). Therefore, judging from the sediment thicknesses, it seems likely that the event horizons that we have identified on the two northern segments of the GSLF are in Holocene sediments as well.

The event horizons identified on Figures 7-10, especially Figure 7 (line 10GSL44), are all possible targets for a coring and dating study similar to the one that we carried out in the south arm. The paleoearthquake dates resulting from such studies would provide estimates of the average recurrence intervals for surface faulting earthquakes on the northern two segments of the GSLF. In the meantime, given the available data, it seems reasonable to assume that the average recurrence interval for large earthquakes on the Rozel and Promontory segments is comparable to that on the Fremont Island and Antelope Island segments (4200 ± 1400 yrs; Dinter and Pechmann, 2005).

ACKNOWLEDGEMENTS

We are grateful to our long-time USGS collaborator, Robert Baskin, and the local USGS Water Resources Office at which he is based, for their generous assistance with the lengthy data collection phase of this project. Paul Roberson of the University of Utah Seismograph Stations (UUSS) used his Geographic Information System (GIS) skills to digitize our fault maps and created the maps in Figures 2-6 of this report. J. Mark Hale of UUSS made the publication quality versions of the seismic reflection sections in Figure 7-10 and assisted with the interpretation of these sections. The IHS Kingdom Educational Grant Program provided licenses for the Kingdom Software package, which greatly facilitated the viewing and interpretation of the seismic reflection data.

REFERENCES

- Baskin, R.L. (2005). Calculation of area and volume for the south part of Great Salt Lake, Utah, *U.S. Geol. Surv. Open-File Rept. 2005-1327*, 6 pp.
- Baskin, R.L. (2006). Calculation of area and volume for the north part of Great Salt Lake, Utah, *U.S. Geol. Surv. Open-File Rept. 2006-1359*, 6 pp.
- Baskin, R.L. (2014). Occurrence and distribution of microbial bioherms, Great Salt Lake, Utah, Ph.D. Thesis, University of Utah, Salt Lake City, Utah, in review.
- Baskin, R.L., and D.V. Allen (2005). Bathymetric map of the south part of Great Salt Lake, Utah, 2005, *U.S. Geol. Surv. Scientific Investigations Map 2894*, scale 1:100,000.
- Baskin, R.L., and J. Turner (2006). Bathymetric map of the north part of Great Salt Lake, Utah, 2006, *U.S. Geol. Surv. Scientific Investigations Map 2954*, scale 1:100,000.
- Bortz, L.C., S.A. Cook, and O.J. Morrison (1985). Great Salt Lake area, Utah, in Gries, R.R., and Dyer, R.C., eds., *Seismic Exploration of the Rocky Mountain region*, R.R. Gries and R.C. Dyer (Editors), Rocky Mountain Association of Geologists and the Denver Geophysical Society, Denver, Colorado, 275-281.
- Colman, S.M., K.R. Kelts, and D.A. Dinter (2002). Depositional history and neotectonics in Great Salt Lake, Utah, from high-resolution seismic stratigraphy, *Sed. Geol.* **148**, 61-78.
- Dinter, D.A., and J.C. Pechmann (2005). Segmentation and Holocene displacement history of the Great Salt Lake fault, Utah, in *Proceedings Volume, Basin and Range Province Seismic Hazards Summit II*, W.L. Lund (Editor), *Utah Geol. Survey, Misc. Publ. 05-2*, CD, 5 pp. (extended abstract).
- Mikulich, M., and R.B. Smith (1974). Seismic reflection and aeromagnetic surveys of the Great Salt Lake, Utah, *Geol. Soc. Am. Bull.* **85**, 991-1002.
- Mohapatra, G.K., and R.A. Johnson (1998). Localization of listric faults at thrust fault ramps beneath the Great Salt Lake Basin, Utah: Evidence from seismic imaging and finite element modeling: *J. Geophys. Res.* **103**, 10,047-10,063.
- Smith, R.B., and R.L. Bruhn (1984). Intraplate extensional tectonics of the eastern Basin-Range: Inferences on structural style from seismic reflection data, regional tectonics, and thermal-mechanical models of brittle-ductile deformation, *J. Geophys. Res.* **89**, 5733-5762.
- Viveiros, J.J. (1986). Cenozoic tectonics of the Great Salt Lake from seismic reflection data, M.S. Thesis, University of Utah, Salt Lake City, Utah, 81 pp.
- Wells, D.L., and K.J. Coppersmith (1994). New empirical relationships among magnitude, rupture length, rupture width, rupture area, and surface displacement, *Bull. Seism. Soc. Am.* **84**, 974-1002.

- Wesnousky, S.G. (2008). Displacement and geometrical characteristics of earthquake surface ruptures: Issues and implications for seismic-hazard analysis and the process of earthquake rupture, *Bull. Seism. Soc. Am.* **98**, 1609-1632.
- White, J.S., S.E. Null, and D.G. Tarboton (2014). Modeled changes to Great Salt Lake salinity from railroad causeway alteration, Final Report to the Utah Division of Forestry, Fire, and State Lands, 19 pp.
- Wong, I., W. Lund, C. DuRoss, W. Arabasz, J. Pechmann, A. Crone, N. Luco, S. Personius, M. Petersen, S. Olig, and D. Schwartz (2011). The working group on Utah earthquake probabilities (WGUEP): Background and goals, *Seism. Res. Lett.* **82**, 345-346.

BIBLIOGRAPHY OF PUBLICATIONS RESULTING FROM WORK PERFORMED UNDER THE AWARD

- Dinter, D.A., and J.C. Pechmann (2004). Holocene segmentation and displacement history of the East Great Salt Lake fault, Utah, *Basin and Range Province Seismic Hazards Summit II, Program and Abstracts*, Reno-Sparks, Nevada, May 16-19, 2004, 82-86 (abstract).
- Dinter, D.A., and J.C. Pechmann (2005). Segmentation and Holocene displacement history of the Great Salt Lake fault, Utah, in *Proceedings Volume, Basin and Range Province Seismic Hazards Summit II*, W.L. Lund (Editor), *Utah Geol. Survey, Misc. Publ. 05-2*, CD, 5 pp. (extended abstract).
- Dinter, D., and J. Pechmann (2012). Paleoseismology of active normal faults submerged beneath the Great Salt Lake, Utah, *AEG News* **55**, 52-53 (invited abstract).

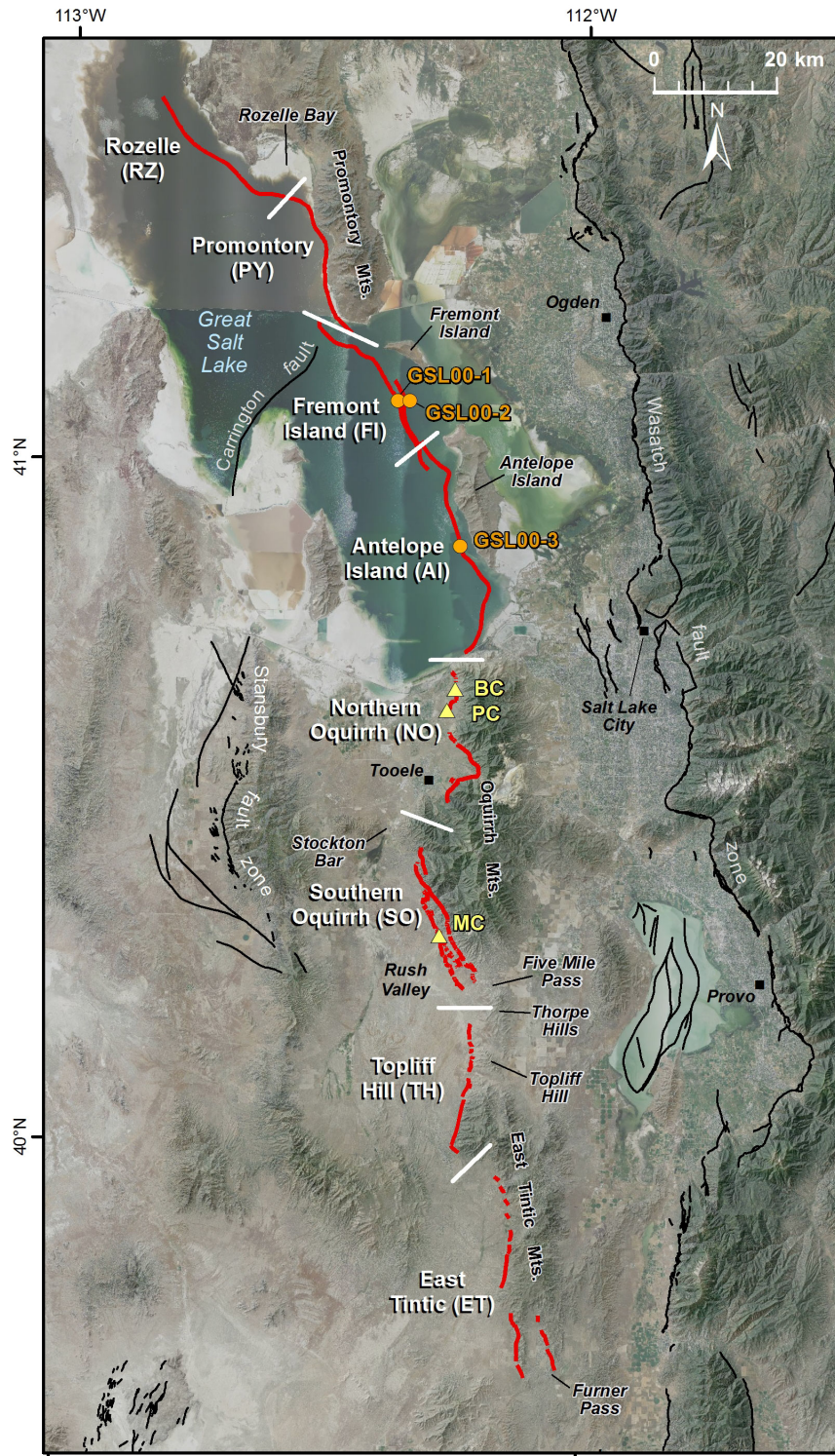


Figure 1. Map of the Oquirrh-Great Salt Lake fault zone (red), interpreted segment boundaries for this fault zone (white bars), and other active faults in the Wasatch Front region of north-central Utah (black). The fault traces shown for the Great Salt Lake fault zone are the ones that are currently in the National Fault Database, and are from our previous studies. This figure was prepared for the Working Group on Utah Earthquake Probabilities by S. Olig of URS Corporation and C. DuRoss and C. Unger of the Utah Geological Survey.

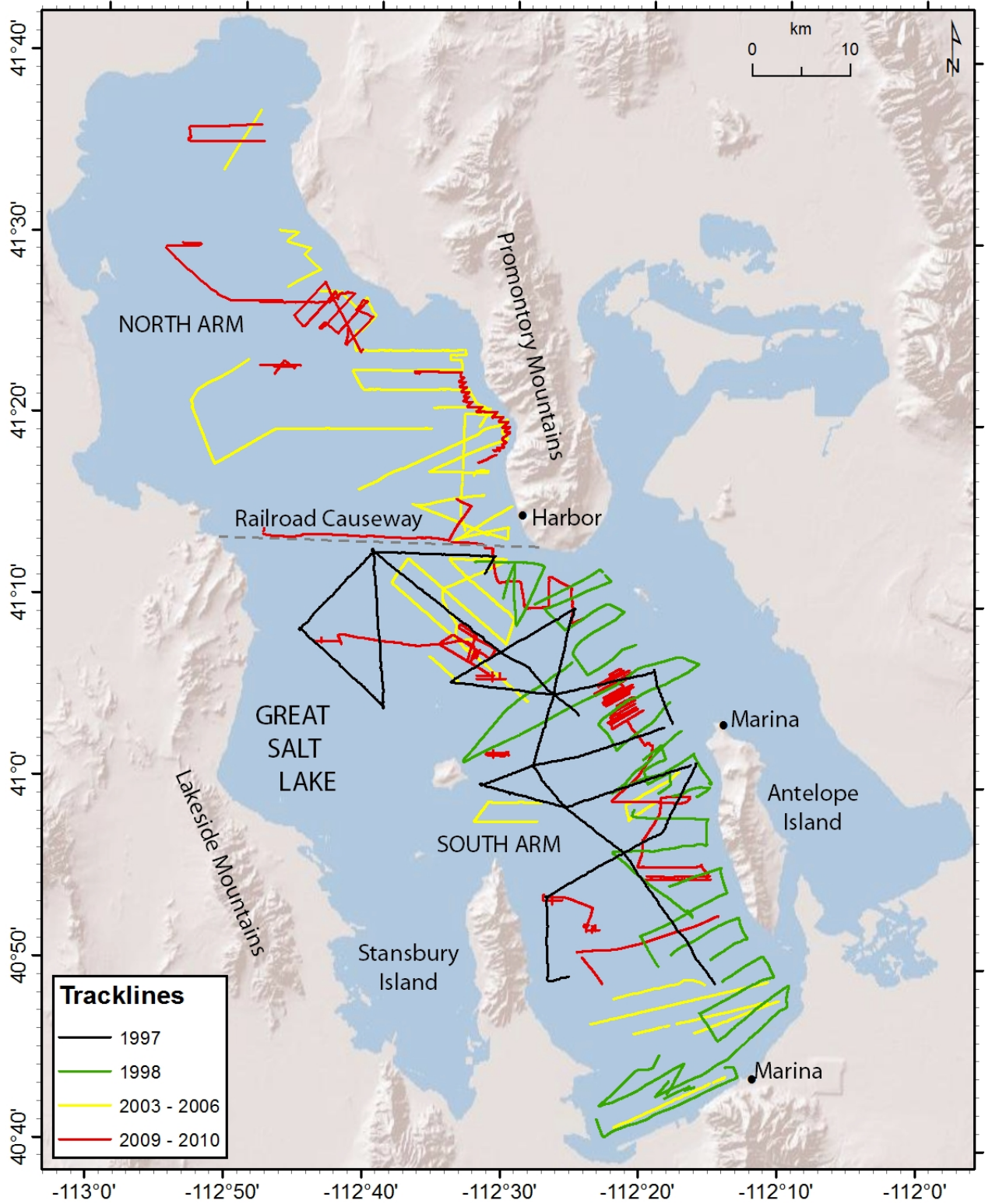


Figure 2. Map of the Great Salt Lake showing the locations of the seismic reflection profiles used in this study. We acquired the 2003-2006 and 2009-2010 data for this study and the 1998 data for a previous study (Dinter and Pechmann, 2005). The 1997 data are from Colman et al. (2002).

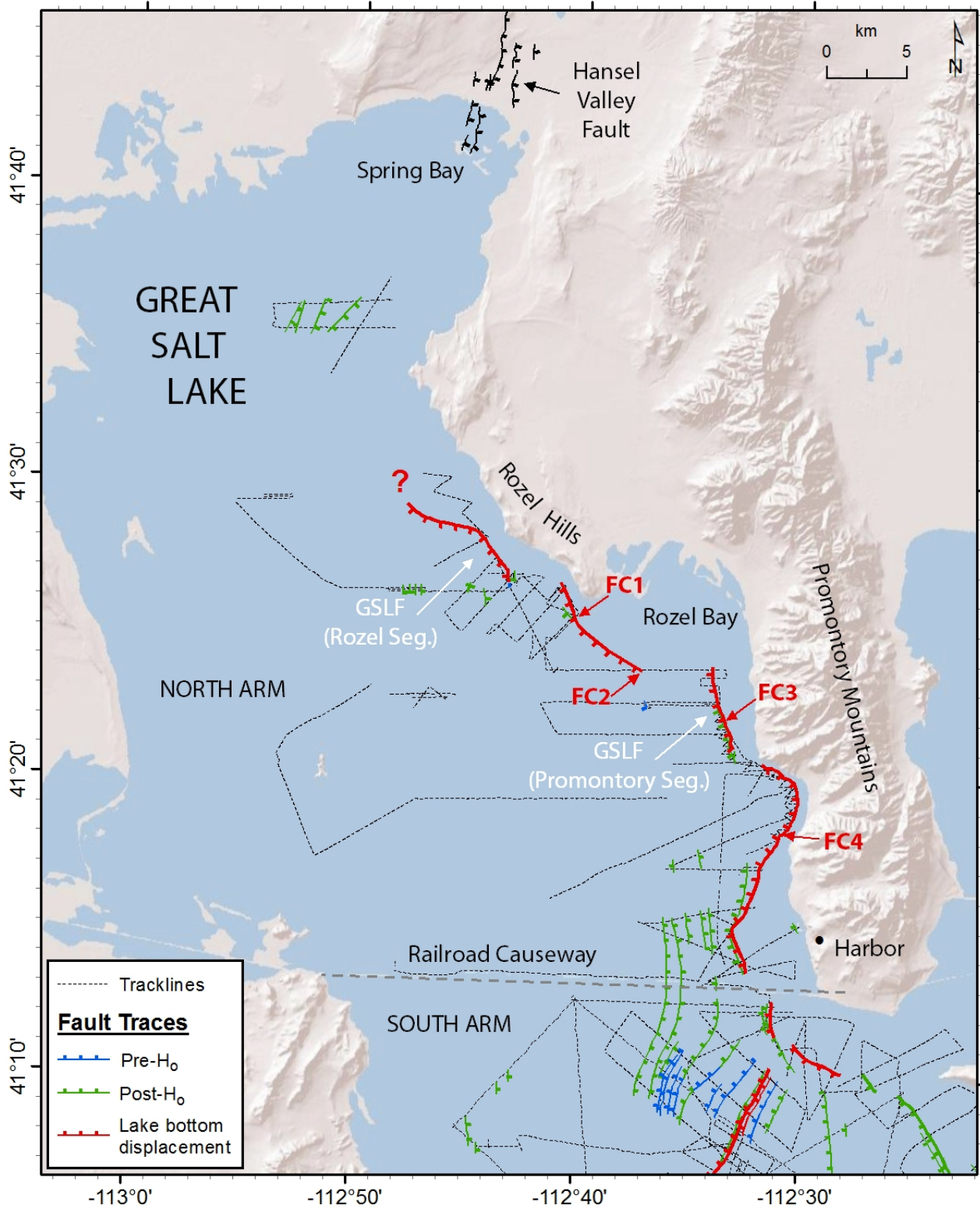


Figure 3. Map showing seismic reflection tracklines and faults in the north arm of the Great Salt Lake. The heavier line widths show the active traces of the Great Salt Lake and Carrington faults.

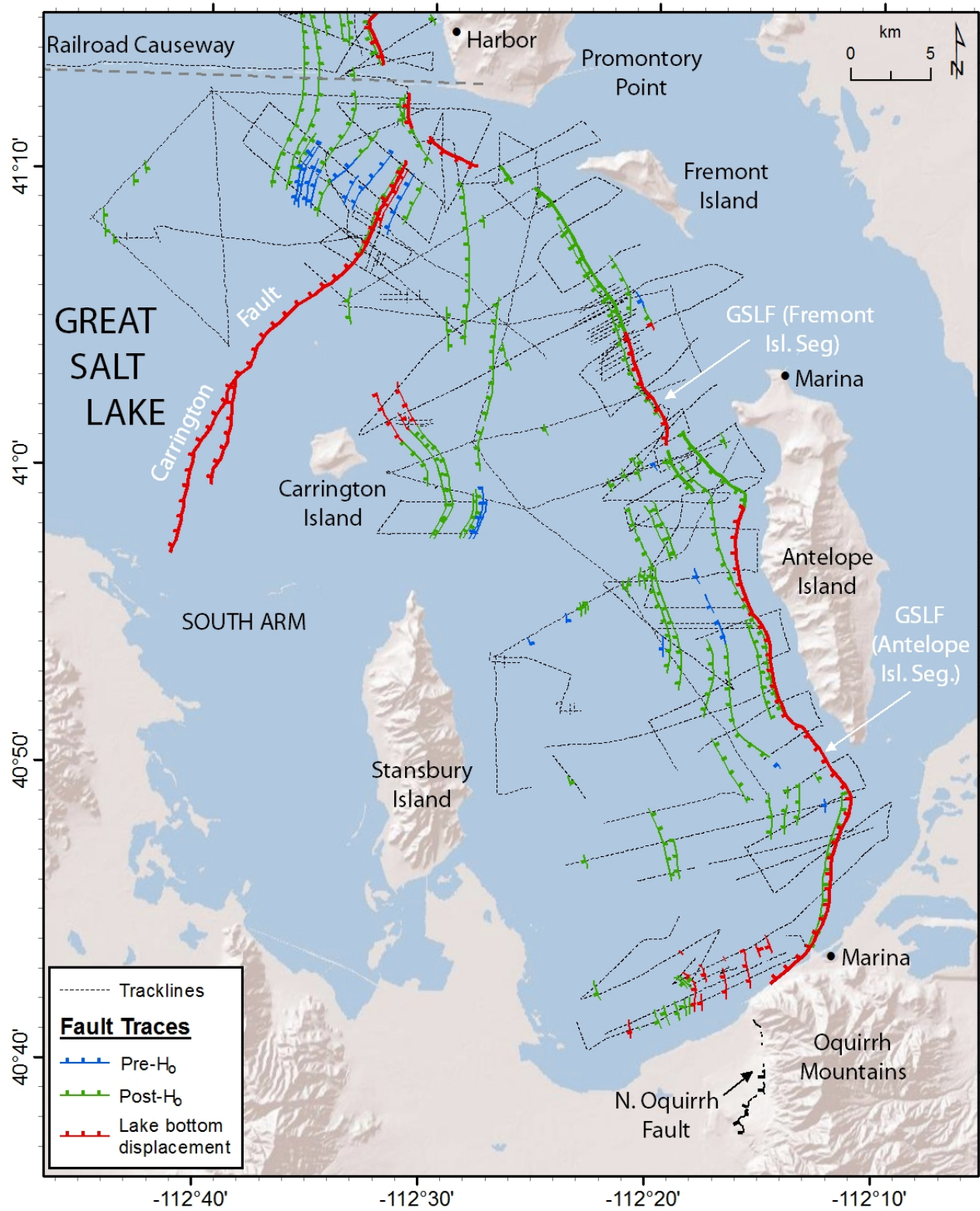


Figure 4. Map showing seismic reflection tracklines and faults in the south arm of the Great Salt Lake. The heavier line widths show the active traces of the Great Salt Lake and Carrington faults.

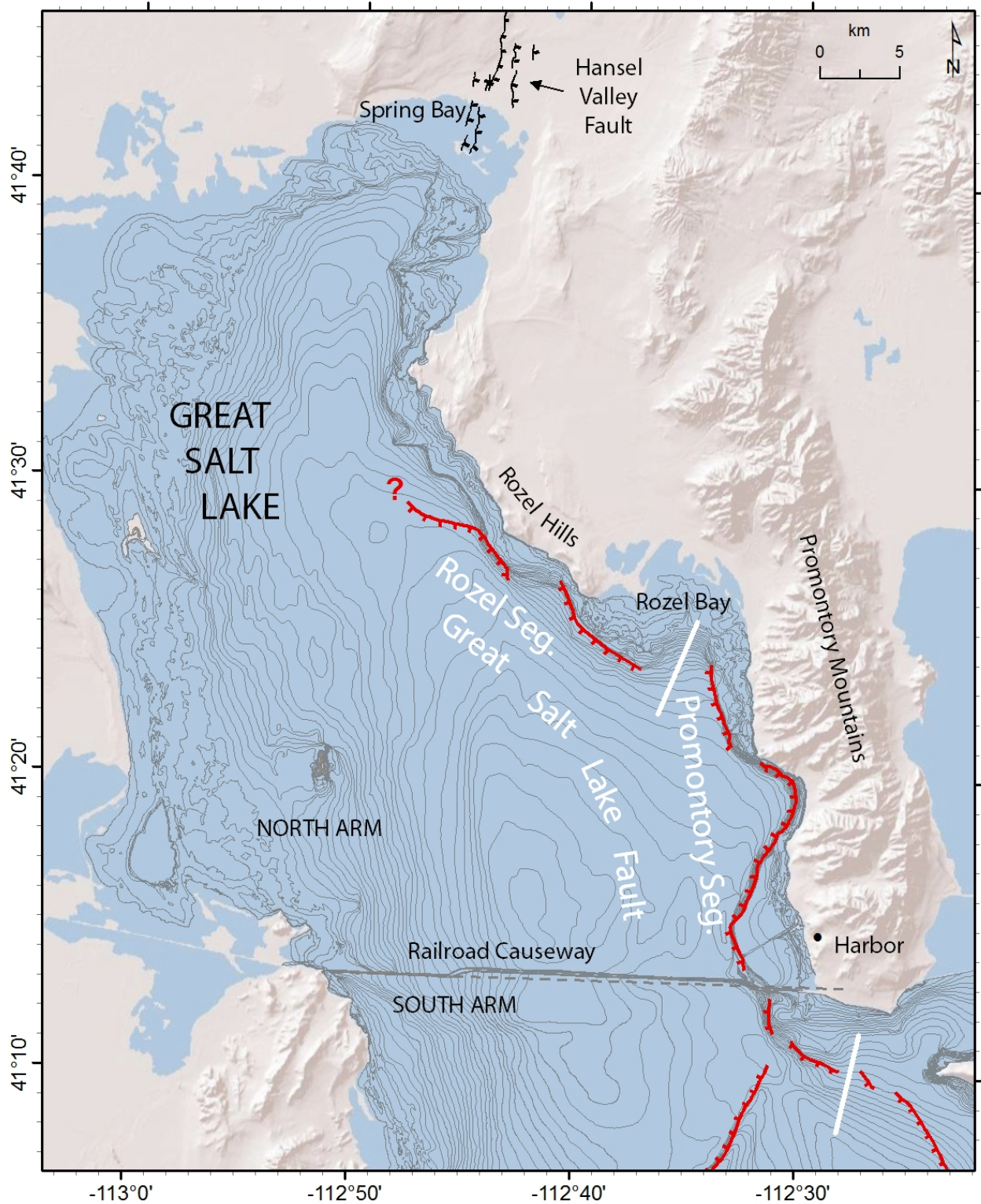


Figure 5. Map of the north arm of the Great Salt Lake showing the active traces of the Great Salt Lake and Carrington faults (red), our proposed segment boundaries for the former (white bars), and bathymetric contours from Baskin and Allen (2005) and Baskin and Turner (2006). The contour interval is one foot, with the shallowest contour at an elevation of 4200'.

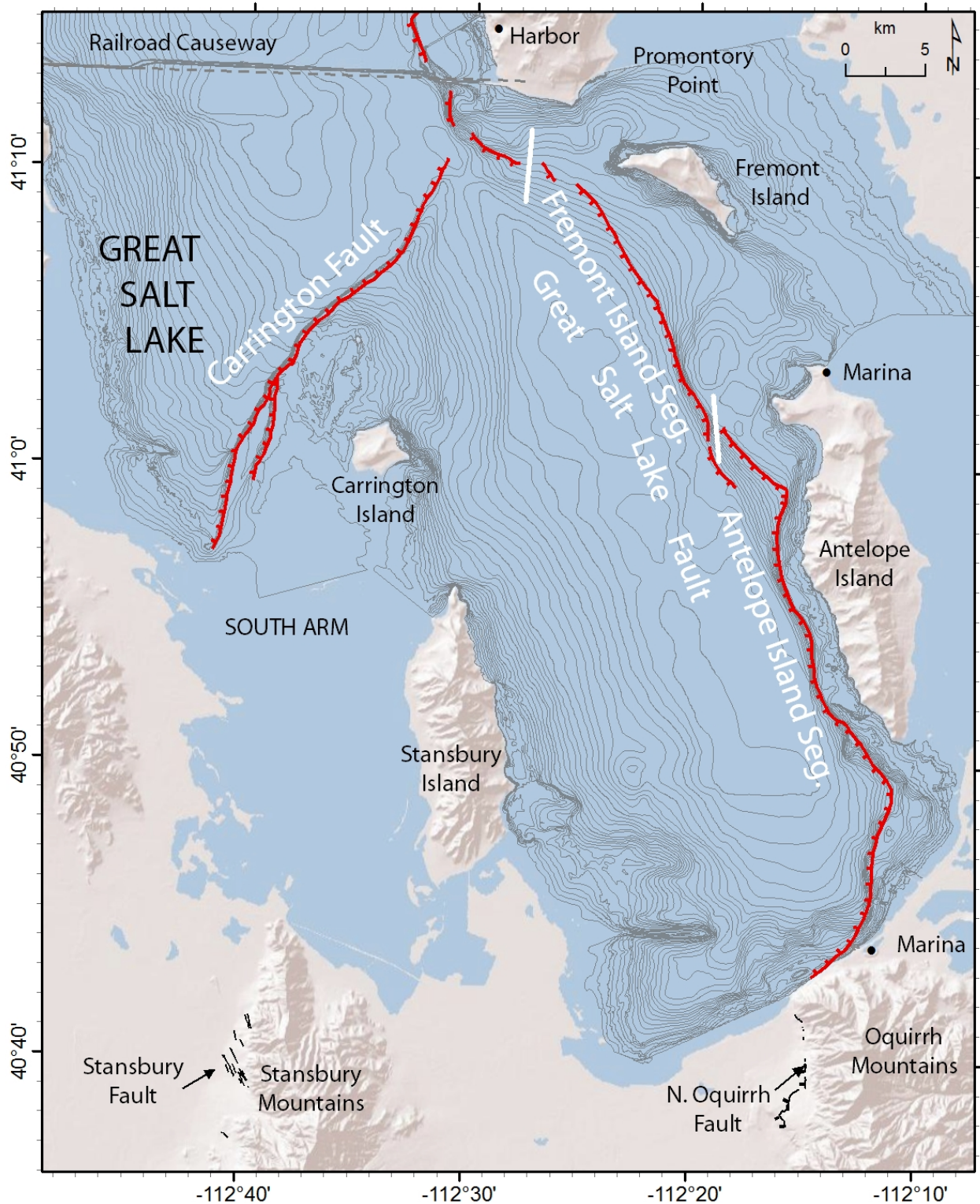


Figure 6. Map of the south arm of the Great Salt Lake showing the active traces of the Great Salt Lake and Carrington faults (red), our proposed segment boundaries for the former (white bars), and bathymetric contours from Baskin and Allen (2005) and Baskin and Turner (2006). The contour interval is one foot, with the shallowest contour at an elevation of 4200'.

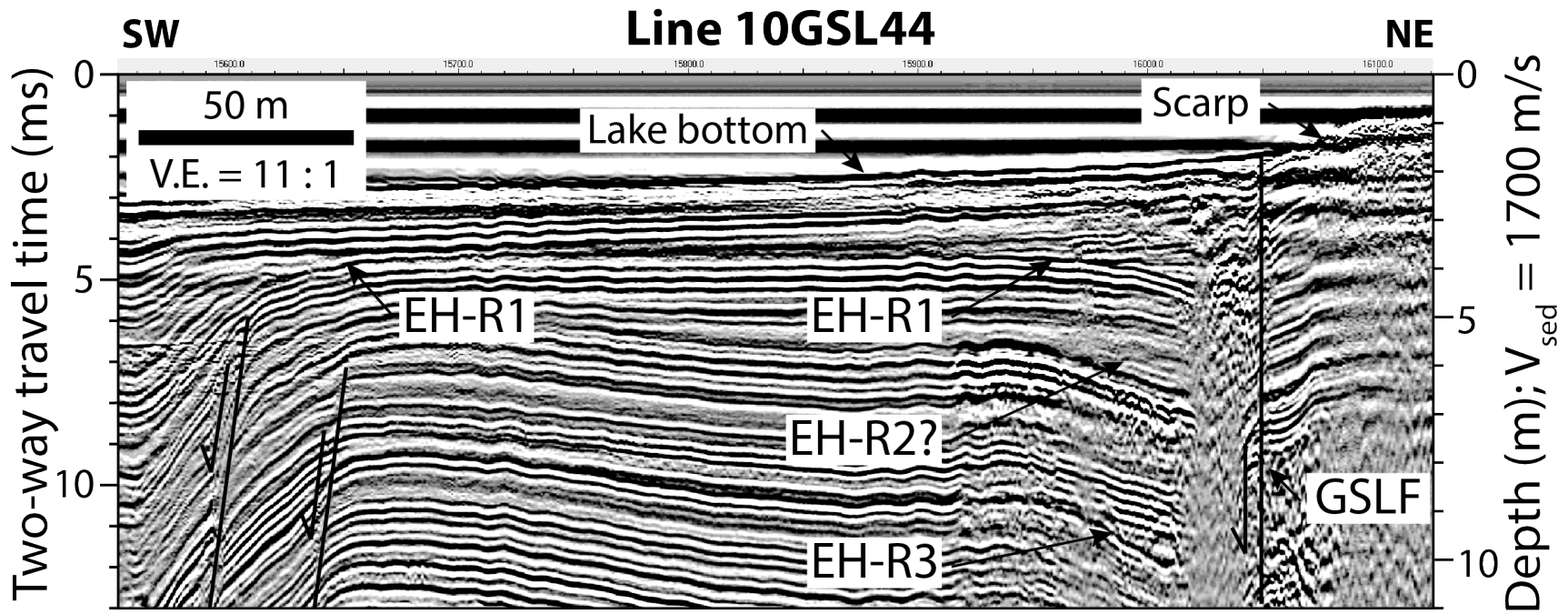


Figure 7. Seismic reflection data from line 10GSL44 where it crosses the Great Salt Lake fault at location FC-1 on Figure 3. EH-R1, EH-R2, and EH-R3 are interpreted earthquake event horizons.

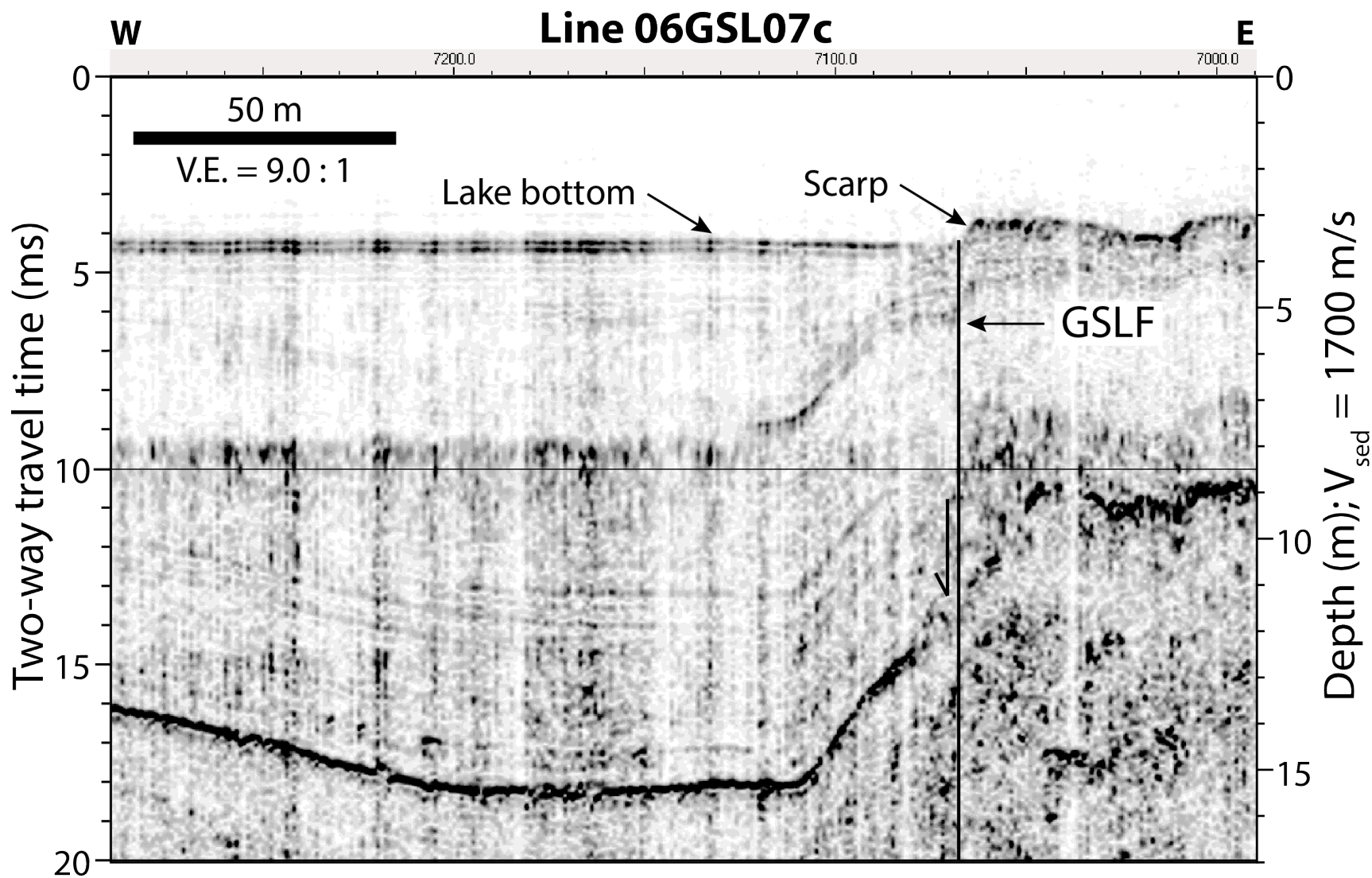


Figure 8. High-frequency Chirp seismic reflection data from line 06GSL07c where it crosses the Great Salt Lake fault at location FC-2 on Figure 3.

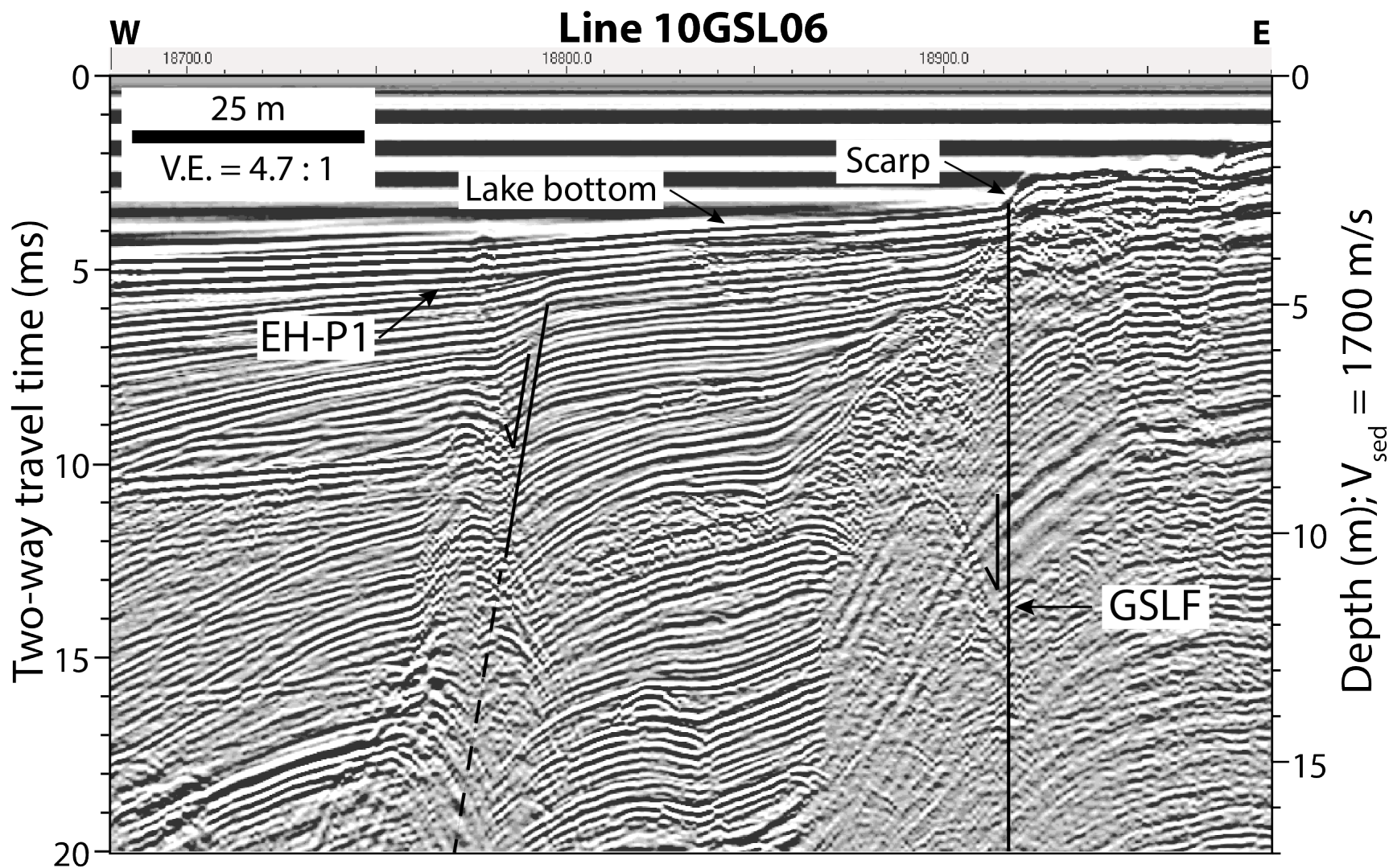


Figure 9. Seismic reflection data from line 10GSL06 where it crosses the Great Salt Lake fault at location FC-3 on Figure 3. EH-P1 is an interpreted earthquake event horizon.

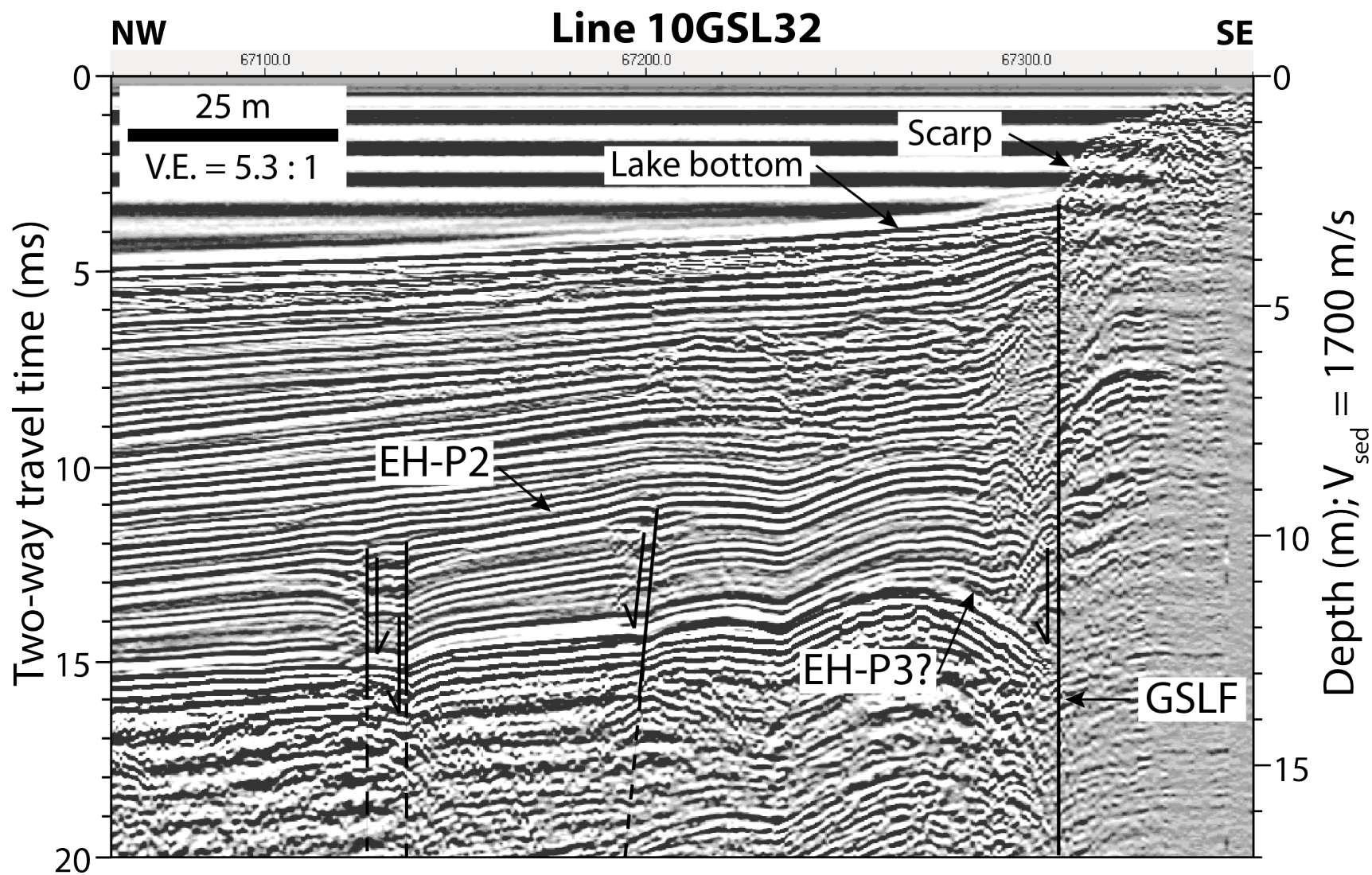


Figure 10. Seismic reflection data from line 10GSL32 where it crosses the Great Salt Lake fault at location FC-4 on Figure 3. EH-P2 and EH-P3 are interpreted earthquake event horizons.